analytical chemistry

Article

Cite This: *Anal. Chem.* 2019, 91, 5841−5849

pubs.acs.org/ac

Robust Bioengineered Apoferritin Nanoprobes for Ultrasensitive Detection of Infectious Pancreatic Necrosis Virus

Sachin Ganpat Chavan,[†,‡] Ajay Kumar Yagati,[†,‡] Mohsen Mohammadniaei,[†] Junhong Min,[*,†] and Min-Ho Lee[*,†]

[†]School of Integrative Engineering, Chung-Ang University, Heuseok-dong, Dongjak-Gu, Seoul 06974, South Korea

Supporting Information

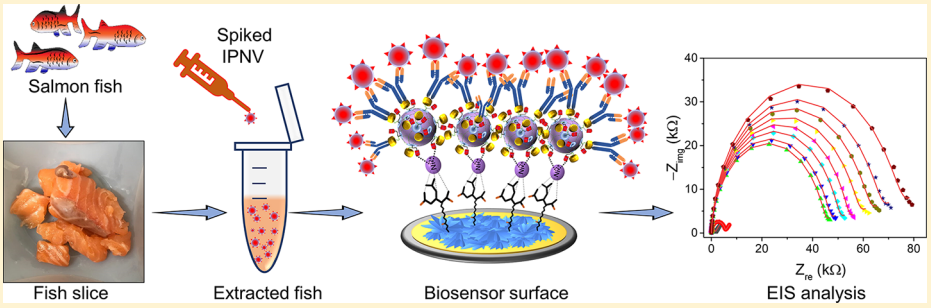

ABSTRACT: Infectious pancreatic necrosis virus (IPNV) has been identified as a viral pathogen for many fish diseases that have become a huge hurdle for the growing fishing industry. Thus, in this work, we report a label-free impedance biosensor to quantify IPNV in real fish samples at point-of-care (POC) level. High specificity IPNV sensor with a detection limit of 2.69 $TCID_{50}$/mL was achieved by conjugating IPNV antibodies to portable Au disk electrode chips using human heavy chain apoferritin (H-AFN) nanoprobes as a binding agent. H-AFN probes were bioengineered through PCR by incorporating pET-28b(+) resulting in 24 subunits of 6 × his-tag and protein-G units on its outer surface to increase the sensitivity of the IPNV detection. The biosensor surface modifications were characterized by differential pulse voltammetry (DPV) and EIS methods for each modification step. The proposed nanoprobe based sensor showed three-fold enhancement in charge transfer resistance toward IPNV detection in comparison with the traditional linker approach when measured in a group of similar virus molecules. The portable sensor exhibited a linear range of 100−10000 $TCID_{50}$/mL and sensitivity of 5.40×10^{-4} $TCID_{50}$/mL in real-fish samples. The performance of the proposed IPNV sensor was fully validated using an enzyme-linked immunosorbent assay (ELISA) technique with a sensitivity of 3.02×10^{-4} $TCID_{50}$/mL. Results from H-AFN nanoprobe based IPNV sensor indicated high selectivity, sensitivity, and stability could be a promising platform for the detection of similar fish viruses and other biological molecules of interest.

Infectious pancreatic necrosis virus (IPNV), a nonenveloped, double-stranded RNA virus that is an etiological agent of an acute contagious disease of several species of freshwater and marine fish and belongs to the genus *Aquabirnavirus* within the family *Birnaviridae*.[1] IPNV affects Atlantic salmon at all stages, especially in young salmonid, causing mortality as high as 70%.[2,3] IPNV causes contagious fish diseases and also responsible for huge economic loses of fishing industry, which is widespread in salmonid hatcheries from the Americas to Europe, Asia, and Australia. IPNV infection becomes persistently infected and is a carrier of the virus for a long period, consequently infecting other susceptible fish.[4,5] The infection of IPNV can cause high mortality in first-feeding and postsmolts, with a mortality range 10%−90% and most influence on young salmon fish.[6,7] The universal antiserum neutralizes IPNV infective dose is 10^2 $TCID_{50}$/mL.[8] Present detection methods involve virus isolation in cell cultures and ELISA based techniques. Thus, a rapid and low-cost detection system is necessary for highly selective determination of IPNV in fish for the advancement of aquaculture and fishing industry. Thus, the present study involves the development of a simple, low-cost, impedance sensor for the rapid detection of IPNV in fish samples.

Therefore, it is essential to develop a simple, sensitive, and economically feasible IPNV testing system for pisciculture. Enzyme-linked immunosorbent assay (ELISA) is a standard diagnostic tool for the detection and identification of a variety of analytes of interest. Various types of ELISA kits are available for the detection of human IgG, IgA, and IgM antibodies to bacterial, viral, and fungal antigens and have potential advantages of being able to provide accurate results with high sensitivity. However, this method has limitations in assay time, sample volume, and difficulty in interpretation between serotypes since low levels of antibody are often undetectable.[9]

Received: January 11, 2019
Accepted: April 2, 2019
Published: April 2, 2019

DOI: 10.1021/acs.analchem.9b00187
Anal. Chem. 2019, 91, 5841−5849

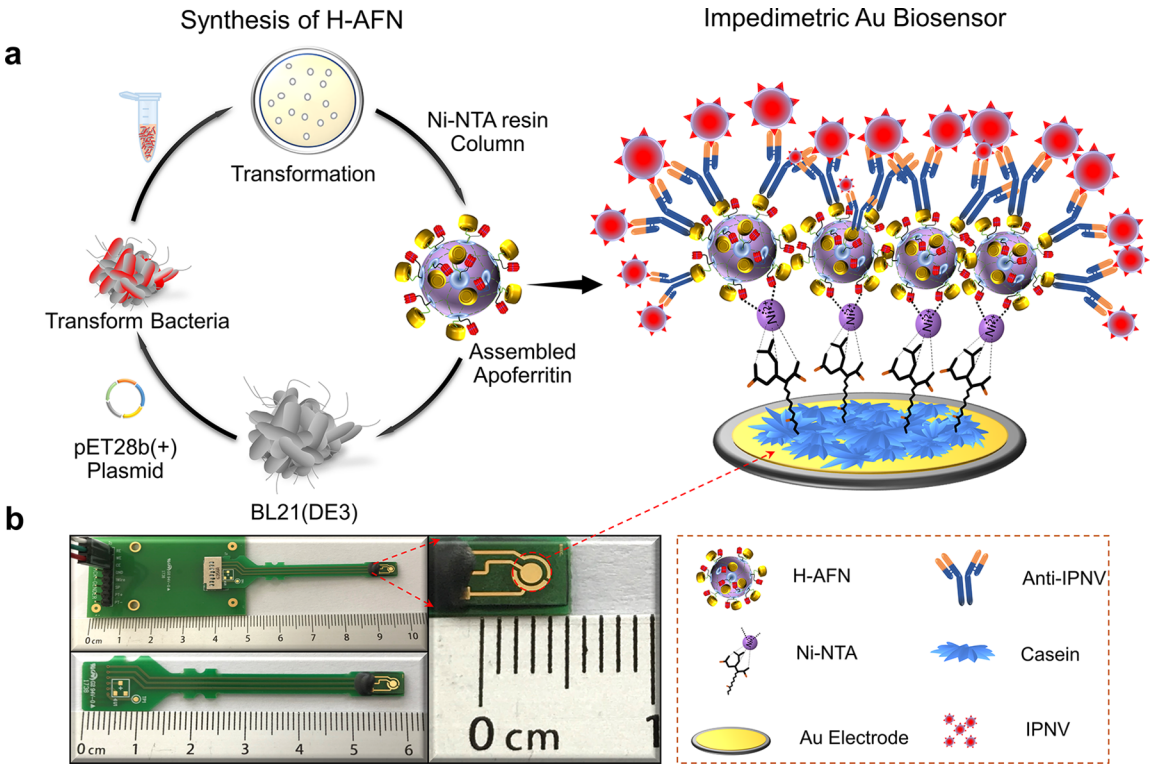

Figure 1. (a) Schematic diagram shows the bacterial transformation, expression, and purification of H-apoferritin and its application toward IPNV detection sensor; (b) optical image of the electrode sensor fabricated on printed circuit board used in a proposed method for EIS and DPV measurements. Magnified view shows Au the three-electrode configuration for working, reference and counter electrodes, respectively.

On the other hand, electrochemical-based methods are becoming promising candidates for the development of label-free biosensors for biomarkers and virus detections. Especially, electrochemical impedance spectroscopy (EIS) offers advantages being mostly destructive and highly sensitive to minute quantities of analytes of interest. The main advantage of the EIS systems relies on their relatively simplistic, having high sensitivity, good selectivity, no limitations on the type of the analyte samples, and simple device configurations, which make them as a potential candidate for determining the concentration of an analyte within a complex sample at the point-of-care (POC) testing for disease diagnostics.[10]

Therefore, POC, miniaturized and highly efficient ways of EIS based detection sensors with more specific ways to quantify the IPNV markers are highly crucial to control and prevention of cancer. Electroanalytical methods such as differential pulse voltammetry (DPV) methods[11] are also promising to obtain increasing sensitivity and selectivity with the detection of biomarkers with tiny sample volumes.[12,13] Recently various biosensing methods for the detection of IPNV were reported; however, direct detection of IPNV in real fish samples by using combined EIS and DPV methods was not reported yet.

Human heavy chain-Apoferritin (H-AFN) composed of hollow cage-like spherical shell structure possess an outer diameter of 12 nm and inner cavity diameter of 8 nm.[14] It is one of the most common bionanomaterials widely used in drug delivery as a probe molecule due to its high stability, integrated structure, and excellent biocompatibility.[15] Further, the outer surface of the protein can easy chemically modulated to bind various enzymes/antibody or metal ions.[16] H-AFN has a unique cavity structure, with efficient binding capabilities for utilizing as a nanoprobe molecule in nanomedicine or biosensor devices.[17] Furthermore, the surface 24 subunits can uniformly be modulated with recombinant technology having excellent biocompatibility and environment for direct binding of enzymes/antibodies with less utilization of chemical linkers enables many potential applications.[18] Each subunit in the H-AFN expressed with protein-G (a cell-surface protein) and 6 × his-tag, which interact with the Fc region of the antibodies and Nickel-nitrilotriacetic acid (Ni-NTA). The presence of protein-G provides directionality to the targeting moiety because protein-G binds with the Fc region of an antibody, which provides proper orientation of antibody in an outward direction and thus rendering the Fab region sterically accessible.[19,20] H-AFN has been adopted for various applications in nanomedicine, drug delivery, and many bioelectronics applications;[21] however, there has been little research that has explored by using this protein for antibody bindings toward IPNV detection in real fish samples.

Thus, herein, we present a portable, low-cost, fast and efficient POC biosensor for IPNV detection in real fish samples. In the present approach, we developed Au disk electrodes on a printed circuit board (PCB) as a sensor chip that integrates with the microSD card readout circuit board utilizing tiny amount of analyte samples. Sensing electrodes were incubated with H-AFN nanoprobes to conjugate IPNV antibodies and further the sensitivity toward IPNV in both phosphate buffer saline (PBS) and salmon fish samples with EIS and DPV monitoring. For both EIS and DPV assays, the IPNV specific antibodies were coupled to H-AFN, and the probe was immobilized on a gold surface via the affinity of its 6 × his-tag to a nickel-chelating nitrilotriacetic acid (Ni-NTA) surface, and for surface blocking casein was adopted. Sensor

DOI: 10.1021/acs.analchem.9b00187
Anal. Chem. 2019, 91, 5841−5849

output parameters such as a limit of detection, sensitivity, linear range, and relative standard deviation were evaluated and further compared with the ELISA method.

2. EXPERIMENTAL SECTION

2.1. Chemical and Reagent. The H-apoferritin gene (FTH1: NM_002032) and cloned pET-28b(+) vector purchased from Gene Script (Hong Kong). The BL21(DE3) competent cells were received from Biolabs (UK). The isopropyl β-D-1-thiogalactopyranoside (IPTG), amino-nitrilotriacetic acid (ANTA), dithiolbis(succinimidyl propionate) (DTSP), EDC/NHS, and Nickel(II)sulfate were from Sigma-Aldrich. Ni-NTA buffer kit, Ni-NTA column, and Ni-NTA HRP-conjugated antibody were purchased from Qiagen (USA). The Dynabeads M-270 were from Thermofisher. SDS-PAGE kit was obtained from Biorad (USA). The anti-6 × his-tag antibody was purchased from Invitrogen (Rockford, USA). The kanamycin sulfate, Ni-NTA His·Bind resin was obtained Merck and Goat antimouse antibody HRP-conjugated acquired from ABClon. The monoclonal capture and detection anti-IPNV-1A#82 (4.43 mg/mL) antibodies and IPNV (8.08×10^4 $TCID_{50}$/mL) were obtained from Bionote (South Korea).

2.2. Apoferritin Purification. The primary material for the purification of human apoferritin heavy chain subunit was genetically cloned into pET-28b(+) vector by standard polymerase chain reaction (PCR) method (see Figure S2, Supporting Information) using primer Forward: GGCCCCAAGGGGTTATGCTAGT and Reverse: GATCCCGCGAAATTAATACG (GenScript, Hong Kong). The pET-28b(+) vector enclosed with H-AFN gene (FTH1, NM_002032), Protein-G and 6 × his-tag were serially inserted by 5′ *Nde*I (CATATG) to *XhoI* (CTCGAG) 3′ restriction sites with a start to stop codon. Briefly, H-Apoferritin gene inserted between *Nde*I to *Bam*HI restriction site, protein-G, and 6 × his-tag were inserted between *Bam*HI to *XhoI* restriction site of C-terminus position. The digested pET-28b(+) vector was heat shock transformed into BL21(DE3) *Escherichia coli* competent cell, on LB agar plate containing kanamycin resistance, then transformed colony was analysis by DNA sequencing (Bioneer, South Korea). The vector expression and induction grew in 50 mL of LB media including 30 mg/mL Kanamycin, incubated at 30 °C to OD_{600} reaching 0.6−1.0. The cells ware induced addition of 0.4 mM isopropyl-β-D-1-thiogalactopyranoside (IPTG) from 100 mM stock solution. After induced cells were harvested and tip sonicated into lysis buffer, the lysate was centrifuged at 10 000 × *g* at 4 °C for 30 min for separate cell debris; clear lysate was collected and excess cell debris discarded. Finally, H-AFN was purified using Ni-NTA His-Bind Resin column from the lysate (Figure 1a) and analyzed by gene sequencing (Bioneer, South Korea), DLS, SDS-PAGE, and TEM image.

2.3. Apparatus and Characterization. First, the purified H-apoferritin nanoparticle absorbance at 280 nm was measured, and the concentration was estimated by BCA assay. The outer surface diameter measured by dynamic light scattering (DLS) zeta sizer (UK). The morphological structure analysis by the TEM image (Zeiss LEO 912 AB) with an operating voltage applied CM-200 kV. The 10 μL H-AFN directly placed on the copper grid for 30-s deposition, and 2% uranyl acetate used for negative staining. Next, we analyzed the molecular size of purified H-AFN on SDS-PAGE electrophoresis under native condition. The 25 μL purified sample was mixed with loading buffer that contained 20 mM Tris-HCl, pH 6.8, 20% glycerol, 0.01% bromophenol blue and heated 95 °C for 5 min; it was then loaded into the gel for 45 min (200 V). Later, the gel was incubated for Coomassie dye staining for 30 min and washed with DPBS until unstained. Protein separated band was visible onto the gel along with size marker. In Western blotting analysis, gel immediately transferred onto the nitrocellulose membrane and was performed applying 4−20% Tris-glycine buffer along with marker; unbound nitrocellulose membrane was blocked with 3% BSA in TBST for 1 h, incubated at room temperature, and then membrane was three times washed with TBST. For H-AFN protein subunits surface expressed for certain protein-G and 6 × his-tag, first antibody as anti-6 × his-tag (1:5000) for 90 min and second antibody as antimouse HRP-conjugated (1:5000) at 60 min were applied, respectively. Then the blot was washed with TBST and processed for super signal west pico chemiluminescent substrate visualized by the ECL detection system.

All electrochemical measurements were carried out using IVIUM CompactStat potentiostat (Eindhoven, Netherlands) on Au-disk electrodes, which were used as a working electrode and the two half-circle ring electrodes acted at the counter and pseudoreference electrodes, respectively (Figure 1b and Figure S6). The EIS performed on Au-disk electrodes in 0.1 M $[Fe(CN)_6]^{3-/4-}$ redox probe with 0.1 M KCl as a supporting electrolyte. Impedance spectra were recorded by applying an AC voltage of 10 mV, with the frequency range of 1 Hz−1 MHz at open circuit potential (equilibrium potential) without any biasing. The obtained impedance spectra were fitted with an appropriate equivalent circuit using commercially available ZView software (Scribner Associates Inc., NC, USA). Differential pulse voltammetry (DPV) was performed at a scan rate of 50 mV/s, having 10 mV pulse amplitude, and 10 ms pulse width in 0.4 to −0.3 V potential window. All potential were referenced with a pseudo Au electrode fabricated on the electrode chip.

2.4. Immunoassay Development. The capture antibody (anti-IPNV) was conjugated to H-AFN via protein-G receptors expressed on the H-AFN surface and subsequently immobilized on the Au-electrode surface via Ni-NTA conjugation reactions between His groups on the surface H-AFN and with the DSP linker present on the Au-electrode.[22] Briefly, Au surface was exposed with 1 mg/mL dithiobis(succinimidyl propionate) (DTSP) in DMSO, which forms a monolayer with Au surface through covalent linkage to the sulfur group. Subsequently, after monolayer formations, the electrodes were rinsed with DMSO and dried under N_2 stream. Next, the electrodes were immersed in 150 mM amino-nitrilotriacetic acid (ANTA) in 0.5 M K_2CO_3 buffer (pH 9.8), which results in amino group reaction with DTSP to form a carboxamide linkage, and excess ANTA was washed out with DI water. Finally, the NTA terminated surface was incubated with 10 mM $NiSO_4$ to ligate the Ni^{2+} ion via the three carboxylates and the tertiary amine of NTA. After rinsing the electrode, the H-AFN having protein-G conjugated with IPNV antibodies in PBS buffer were added onto the electrodes and incubated for 1 h; H-AFN with 6 × his-tag adsorbs to the Ni-NTA moiety via the coordination of the nitrogen of the two of imidazole side chains of the 6 × his-tag. After formations, excess solutions were removed by washing with buffer. For nonspecific bindings, the anti-IPNV functionalized electrodes were immersed in casein 5 ng/mL for 1 h. All steps to construct the IPNV detection surface were characterized by its respective

DOI: 10.1021/acs.analchem.9b00187
Anal. Chem. 2019, 91, 5841−5849

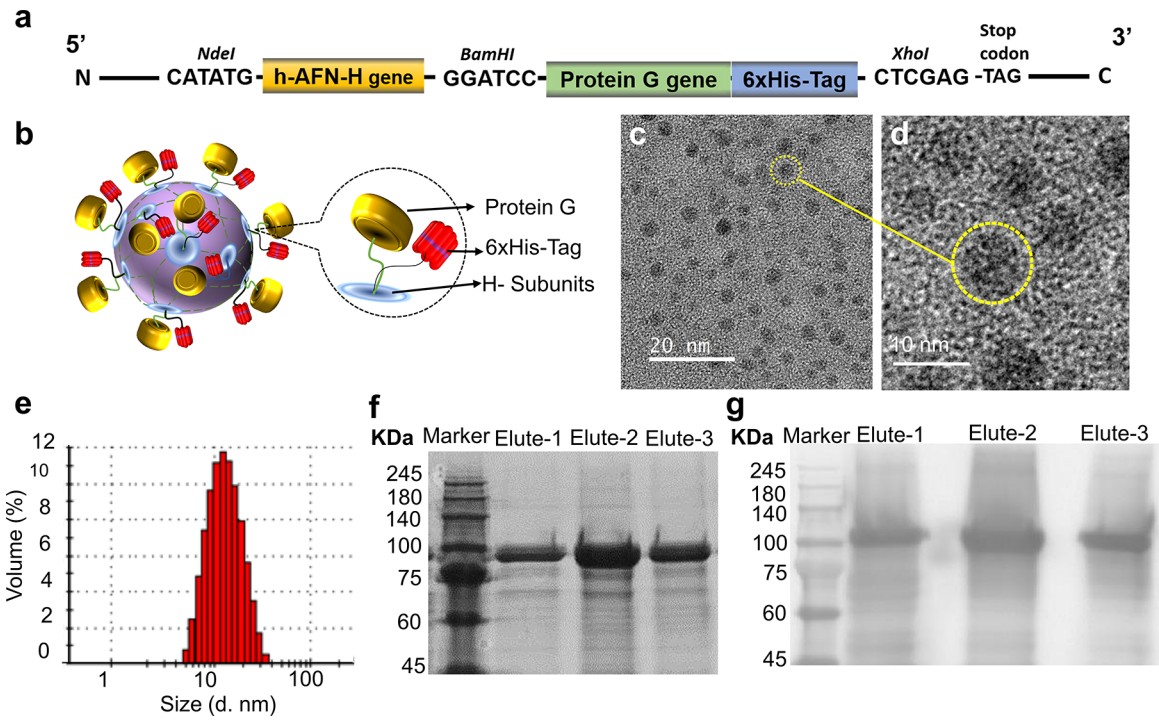

Figure 2. Construction and characterization of H-apoferritin. (a) pET-28b(+) vector genetically constructed by Human-Apoferritin Heavy chain, protein-G, and 6 × his-tag gene. (b) Each H-AFN 24 subunit of heavy chain surface expression with the fusion protein, the main purpose of this expression are protein-G and 6 × his-tag interaction with antibody and Ni-NTA functionalization, respectively. (c, d) TEM Image of purified H-AFN with a spherical shape. (e) DLS analysis, surface size measurement of H-AFN with diameter ~13 nm. (f) Purified H-AFN SDS-PAGE analysis separated on their sequence having a molecular weight of 86 kDa. (g) Western blotting result of purified H-AFN first antibody anti-6 × his antibody used for surface expressed 6 × his-tag and antimouse antibody used for Protein-G.

changes in EIS and DPV measurements. The detailed method for forming the sensor recognition layers on the Au-disk electrode was represented in (Figure 1b).

2.5. Comparison with ELISA. The comparison of ELISA method was performed similarly as the common nanoparticle-based sandwich ELISA.[23] In this test, we used two monoclonal IPNV antibody of which one was anticapture IPNV and antidetection IPNV. First, anticapture IPNV is functionalized surface of the magnetic bead COOH group activated with 40 mM EDC/NHS in 100 mM MES buffer (pH5.0) and second antidetection IPNV conjugated onto the H-AFN nanoprobe surface via protein-G. Then 100 μL of IPNV was added with respective concentration (10^4 to 10° $TCID_{50}$/mL) into the magnetic bead solution mixture after 1 h, incubation at room temperature. The unbounded virus mixture separated using the magnetic bar and three times washed with DPBS. H-AFN Nanoprobe was added into the IPNV conjugated magnetic bead solution mixture for 1 h, starting incubation, and then the virus conjugated to nanoprobe solution was separated similarly suing magnet. Next, again conjugated solution was three times washed with DPBS. Finally, the washed solution was transferred to 96-well plates with respective concentration, and we added the Ni-NTA HRP conjugated antibody, which was bound to H-AFN nanoprobe surface expressed via 6 × his-tag residue. Finally, 100 μL of TMB substrate solution A and B was added to each well and plate was incubated 30 min. Then the plate was analyses under microplate reader absorbance at 450 nm.

2.6. Real Salmon Fish Study. The salmon fish was obtained from the local fish market (Seoul, South Korea) and cleaned with deionized water; 10 g of the fish slices was prepared in the laboratory using a surgical knife and crushed in mortar grander for 15 min. From the crushed slice, we extracted fish oil by centrifugation at 10 000 rpm for 30 min; then the supernatant oil suspension was collected. The fish oil sample prepared into the 100 mM Tris-buffer (pH 8) because the tris-buffer maintained stability and solubility of extracted fish oil. After on 100 μL, corresponding concentrations of IPNV (8×10^4 to $8 \times 10^\circ$ $TCID_{50}$/mL) were spiked in the 100 μL real fish oil, and solution mixture was incubated for overnight, at 4 °C. Finally, the sample was tested on the Au surface for developing IPNV electrochemical sensor.

3. RESULTS AND DISCUSSION

3.1. Characterization of Apoferritin Probes. H-AFN nanoprobes were synthesized for the identification of biological and clinical pathogenic analyst in vivo effects of various biological living organism or cells. The H-AFN have composed 24 subunits, which are heavy and light chain subunits. The H subunits are genetically modified with two adapters unites expressed on protein surface of C terminal site, which interacts with antibody and Ni-NTA.[20] The protein-G commonly binds with target Fc region of antibodies as well as 6 × his-tag and strongly interact with Ni-NTA functionalized derivatives, and the gene sequencing analysis of H-AFN production was presented in Figure S1 (Supporting Information). Here we developed a genetically expressed H-AFN nanoprobe to utilize and for the detection of the highly sensitive salmon fish virus. The constricted pET-28b(+) vector transformation, expression, and induction in *E. coli* bacteria were purified self-assembled H-AFN nanoprobe using Ni-NTA column with the surface expressed protein-G and 6 × his-tag shown in Figure

DOI: 10.1021/acs.analchem.9b00187
Anal. Chem. 2019, 91, 5841−5849

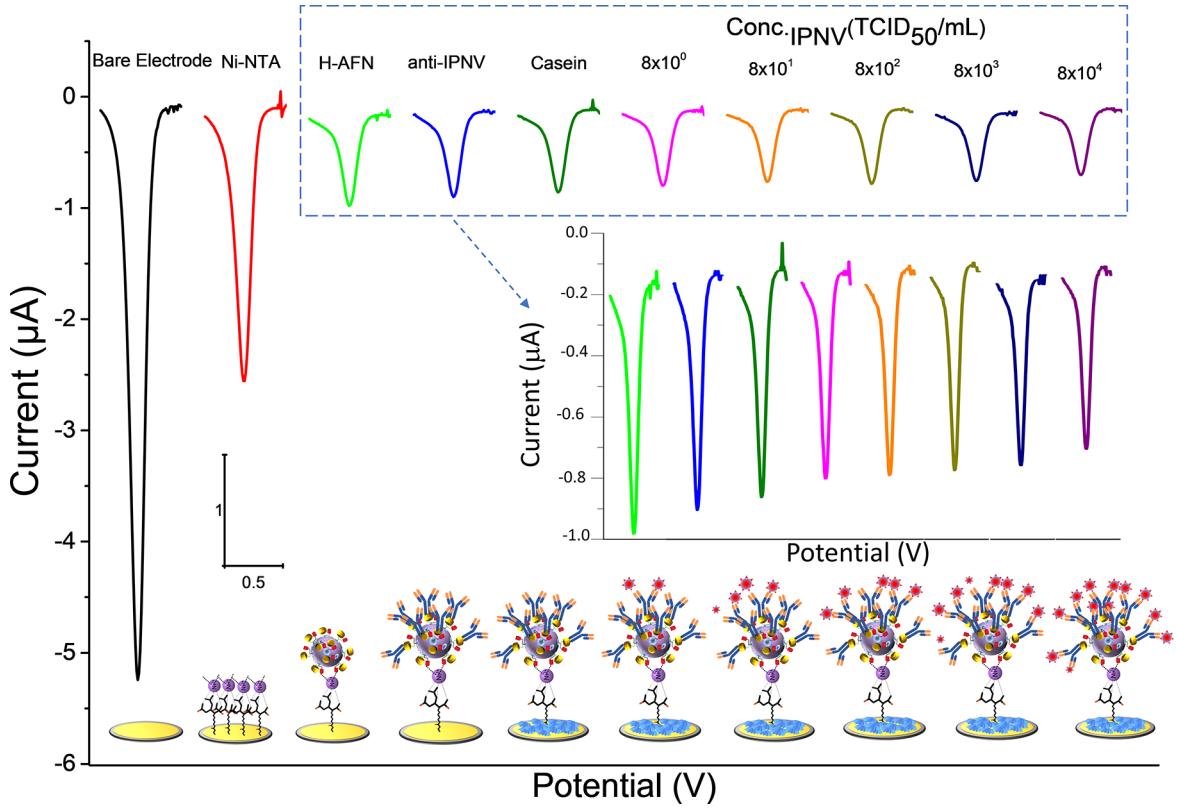

Figure 3. Differential pulse voltammetry recorded during the SAM formation of Ni-NTA (10 mM); H-AFN (1 mg/mL); anti-IPNV (10 mg/mL); casein (5 ng/mL); and different IPNV virus concentrations on Au-electrode sensor. The marked graph in the inset shows a magnified view of the DPV curve.

2a,b. The purified protein analyses successfully matched with gene sequencing data; outer surface size of 12−13 nm measured by dynamic light scattering and TEM (transmission electron microscopy) image indicated the spherical shape (Figure 2c,d,e). The H-AFN purification single band separated was observed on SDS-PAGE gel electrophoresis on their molecular sequence; 86 kDa size was analyzed with the standard marker. Elution lines 2 and 3 optimized large amounts of protein (Figure 2f). Finally, we confirm the purified H-AFN by Western blot, reported the H-AFN surface successfully expressed protein-G and 6 × his-tag using specific antibodies such as antimouse and anti-6 × his-tag antibody, respectively (Figure 2g).

3.2. DPV Characterization for IPNV Bindings on Au-Disk Electrodes. Differential pulse voltammetry (DPV) as an analytical tool offers advantages over other electrochemical techniques as being sensitive to the relatively short pulse time (increases the measured current) and its differential nature (minimizes the charging current), allowing direct analysis at the parts per billion, and is thus preferred for the precise measurement of analyte signals at high sensitivity.[24] The currents were recorded for each modification step performed on the electrode to observe the overall conductivity of the electrode. In Figure 3, the DPV measurements revealed maximum peak current (−5.26 μA) for bare Au electrode; incubation with Ni-NTA on Au resulted in a current of −2.5 μA and subsequent immobilization with H-AFN further reduced to −0.98 μA. Likewise, there is a substantial decrease in current generated upon each modification with SAM formations and gradual decrement with subsequent IPNV antibody−antigen binding interactions. The reduction in the peak currents from DPV clearly indicates inhibition of ions move toward the SAM layers and antigen, which was captured on the electrode surface that quenches the $[Fe(CN_6)]^{3-/4-}$ redox transformation reaction.

3.3. Impedance-Based IPNV Sensor Characterization and Quantification. Electrochemical impedance spectroscopy (EIS) enables the understanding of the electrode−electrolyte kinetics of multiple electrochemical processes as well as information on the capacitance of the system.[25] Therefore, the Nyquist and Bode plots were recorded to examine surface modification for the detection of IPNV in PBS (Figure 4a,b) and in salmon fish samples (Figure 4c,d), respectively. The inset Figure 4a shows an equivalent circuit model used for fitting the experimental results. The bare Au-electrode displayed typical characteristics, where at high frequencies (10^6 to 10^5 Hz), the total impedance is governed by the ohmic resistance of the electrolytic solution (R_s), and thus the phase is close to 0°, and in the mid (10^5 Hz to 10^3 Hz), and the lower frequency region (10^3 to 1 Hz) a combination of capacitive characteristics in parallel with charge transfer resistance (R_{ct}), and diffusion impedance (Z_w) were observed. The capacitive interfacial electrode impedance can be modeled as a constant phase element (CPE) impedance $1/[\text{CPE-T}.(i\omega)^n]$ (where i is the imaginary unit, and ω is angular frequency).[26] Similarly, the Ni-NTA coated electrodes showed higher values in impedance, where R_s was dominant from 10^6 to 10^5 Hz and in midfrequency region 10^5 to 10^3 displayed CPE characteristics along with R_{ct} and diffusion in the low-frequency region. The overall increase in impedance magnitude (|Z|) is due to the insulating characteristics of the SAM-coated surface. Similarly, subsequent treatment with H-

DOI: 10.1021/acs.analchem.9b00187
Anal. Chem. 2019, 91, 5841−5849

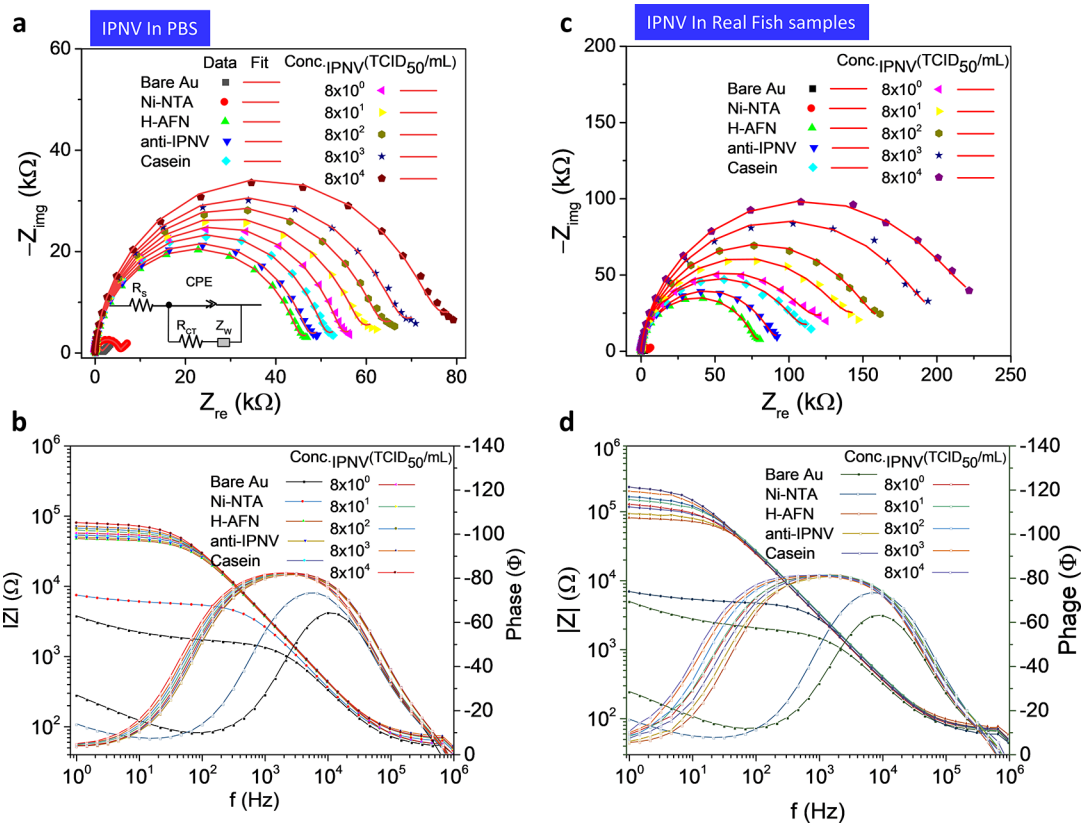

Figure 4. Nyquist plot representing variations in Z′ versus −Z′′ observed from the sensor surface modification and for different concentrations of IPNV ranging from 8⊆10° to 8⊆10^4 $TCID_{50}$/mL in (a) 10 mM PBS (pH 7.0) and (c) salmon fish samples; (b, d) corresponding Bode plots observed for the same Nyquist representations. Panel a inset shows the modified Randle's circuit used for fitting the experimental data obtained for both PBS and real fish samples.

AFN inhibited the movement of $[Fe(CN)_6]^{3-/4-}$ ions toward the electrode; thus, |Z| further increased, and only the CPE and R_{ct} appeared. Similarly, the bindings of anti-IPNV, blocking with casein, and bindings of virus (IPNV) further behave an insulating layer and thus prevent the movement of $[Fe(CN)_6]^{3-/4-}$ ions toward the electrode. This process of virus bindings dramatically enhances an increment in R_{ct} in the spectra. The observed Nyquist plots in both PBS and fish samples for IPNV detection were fitted with modified Randle's equivalent circuit[27] (inset of Figure 4a), which are well in agreement with the model, and the extrapolated circuit elements were presented in Tables 1 and 2 (Supporting Information), respectively. Both tables clearly showed increased values in R_{ct}, however no significant changes in CPE and R_s.

Scan potential window was 0.3 to −0.3 V and observed in 10 mM $[Fe(CN)_6]^{3-/4-}$ and 0.1 M KCl as supporting electrolyte, the inset shows the magnified view of the DPV curves from H-AFN to 8 × 10^4 $TCID_{50}$/mL.

The detection of various concentrations of IPNV ranging from 8 × 10° to 8 × 10^4 $TCID_{50}$/mL was evaluated by observing the changes in the impedance magnitude with the anti-IPNV/Casein/Au-disk electrodes. The normalized impedance magnitude (ΔZ) was evaluated as follows;

$$\Delta Z = (|Z|_{\text{IPNV virus}} - |Z|_{\text{anti-IPNV}})/|Z|_{\text{anti-IPNV}} \quad (1)$$

The measured change in impedance (ΔZ) spectra were recorded and found to increase with increasing IPNV concentration in PBS and fish samples, as shown in (Figure 5a,b), respectively. The response clearly showed that in the low-frequency region (1−100 Hz) a significant change in ΔZ was observed, which was due to the interaction of IPNV. Change in impedance magnitude at 5 Hz ($\Delta Z_{\text{at 5 Hz}}$) was chosen as an analytical parameter and variation at 5 Hz recorded for each addition of IPNV. For determining the sensitivity and detection limit of the developed sensor, a calibration curve method was utilized for the change in impedance magnitude for various concentrations of IPNV in PBS, and fish samples were presented in Figure 5c. The calibration curve was fitted using a standard four-parameter logistic equation according to the following formula,[26] and its standard form is known as B/B_0:[28]

$$y = A_2 + \left[\frac{(A_1 - A_2)}{1 + \left(\frac{x}{EC_{50}}\right)^b}\right] \quad (2)$$

$$\frac{B}{B_0} = \frac{1}{1 + \left(\frac{x}{EC_{50}}\right)^b} \quad (3)$$

Here, y is impedance magnitude (|Z|), x is a concentration of IPNV in $TCID_{50}$/mL, A_1 and A_2 are the minima and maximum analytical response, b represents the slope of inflection point, and EC_{50} is the concentration leading to 50% of the maximum signal, $dy = (A_1 - A_2)\, dB/B_0$ respectively. The best fit values of the experimental data measured in PBS were $y = 0.001 + (0.50967-0.001)/(1 + (x/2285)^{0.7})$, with a correlation

DOI: 10.1021/acs.analchem.9b00187
Anal. Chem. 2019, 91, 5841−5849

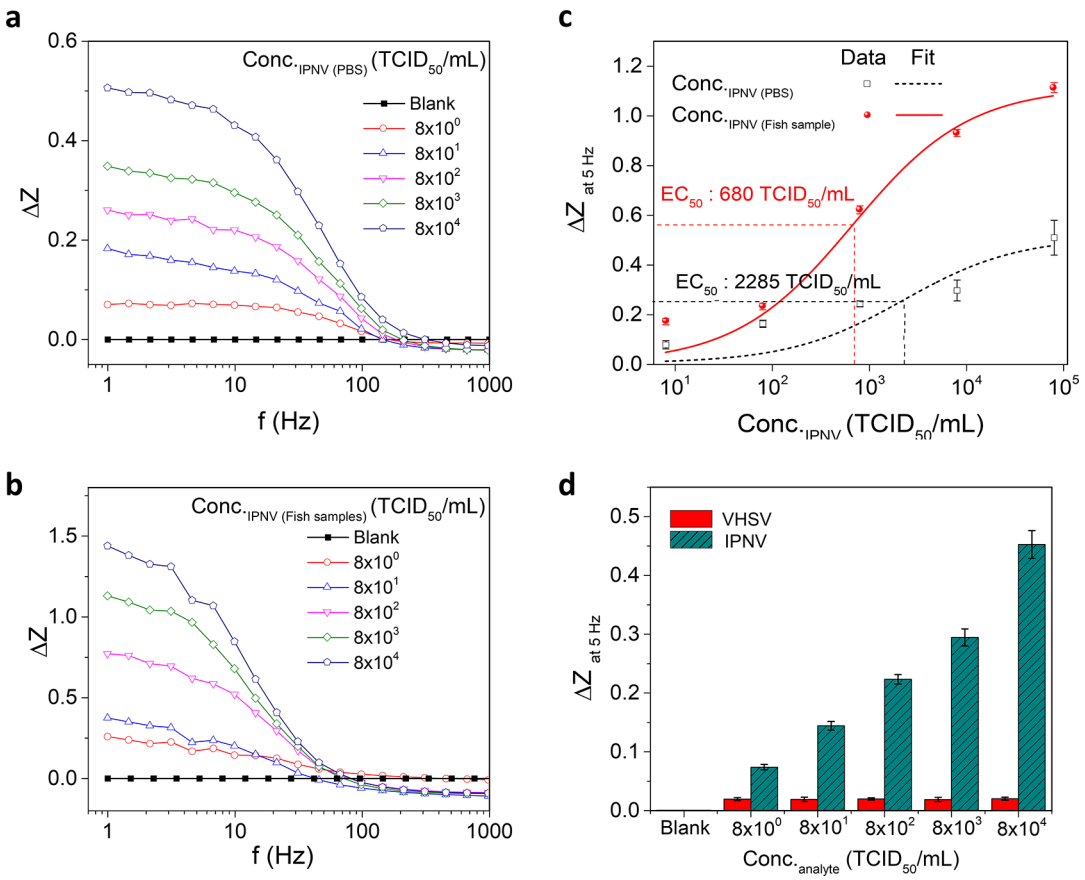

Figure 5. Normalized impedance spectra (ΔZ) obtained for different concentrations of IPNV virus in (a) PBS and (b) fish samples for various concentrations ranging from 8⊆10° to 8⊆10^4 $TCID_{50}$/mL presented over a frequency range of 1 Hz to 1 kHz. (c) Calibration curve for IPNV sensor in both PBS and fish samples at ΔZ at 5 Hz; data points are expressed as mean ± SD of four replicated measurements, and the fitted curve represents the logistic four-parameter regression. (d) Change in impedance observed at 5 Hz with different concentration of the analyte (VHSV and IPNV) on the sensing electrodes.

coefficient of R^2 = 0.998, EC_{50} of 2285 $TCID_{50}$/mL, and a limit of detection (LOD) of 2.69 $TCID_{50}$/mL. Similarly, the best fit values for the experimental data measured in fish samples were $y = 0.001 + (1.11367-0.001)/(1 + (x/680.30)^{0.73})$ with a correlation coefficient of R^2 = 0.998, EC_{50} of 680.30 $TCID_{50}$/mL, and having detection limit of 3.07 $TCID_{50}$/mL. The following formula calculated the LOD = $\frac{Sd / (A_1 - A_2)}{0.13}$, where Sd is the standard deviation of the response.[28] The detection limit was lower than the previous reported IPNV sensors developed by different methods for IPNV detection as shown in Table 3 (Supporting Information). Further, the developed sensor showed a linear range of 100−10000 $TCID_{50}$/mL in both PBS and real fish samples. Also, the repeatability of the IPNV biosensor was tested using four inter- and intraday replicate measurements of a 1000 $TCID_{50}$/mL solution in fish samples wherein the relative standard deviations obtained were 5% and 7%. Thus, assay results indicate that sensor possess acceptable precision for biological assay.[29]

3.4. Selectivity, Stability, and Reproducibility of Developed IPNV Sensor. The capability of the biosensor in discriminating members of IPNV family was evaluated by analyzing similar fish VHS virus compared with analogous concentrations of IPNV (8 × 10° to 8 × 10^4 $TCID_{50}$/mL). No significant changes were observed when VHSV samples were applied to the sensing system (see in Figure S4, Supporting Information). However, substantial changes in $\Delta Z_{\text{ at 5 Hz}}$ were observed for IPNV samples as shown in Figure 5d. Thus, the analyte does not interfere with the sensor's ability to detect IPNV selectively. The findings indicated that the developed sensor is selective in the IPNV in a manner that is not affected by the presence of another virus of similar molecular weight. Further, by performing a parallel experiment, we compared the sensitivity of the developed sensor using H-AFN nanoprobes with the traditional method of antibody bindings Au-electrodes through chemical linker by measuring EIS data. Same concentrations of anti-IPNV (10 μg/mL) and virus (8 × 10^2 $TCID_{50}$/mL) were adopted in both methods. The Nyquist and Bode plots show more significant value in R_{ct} for H-AFN nanoprobes as compared with anti-IPNV bound on bare Au-electrode; this is obvious due to many binding sites available on H-AFN surface modified Au-electrodes (Figure 6a,b). The relative change in the enhancement (RR%) for both binding mechanisms such as an antibody with a chemical linker and H-AFN nanoprobe was calculated using eq 4:

$$RR\% = \left(\frac{R_{\text{virus}} - R_{\text{ab}}}{R_{\text{ab}}}\right) \times 100 \quad (4)$$

Where R_{virus} is the R_{ct} value of the given concentration of the IPNV virus, and R_{ab} is R_{ct} of antibody. It is found that *RR*% after the binding of the virus was observed to be 23% and 8% for H-AFN nanoprobe and linker, respectively (represents 3-

DOI: 10.1021/acs.analchem.9b00187
Anal. Chem. 2019, 91, 5841−5849

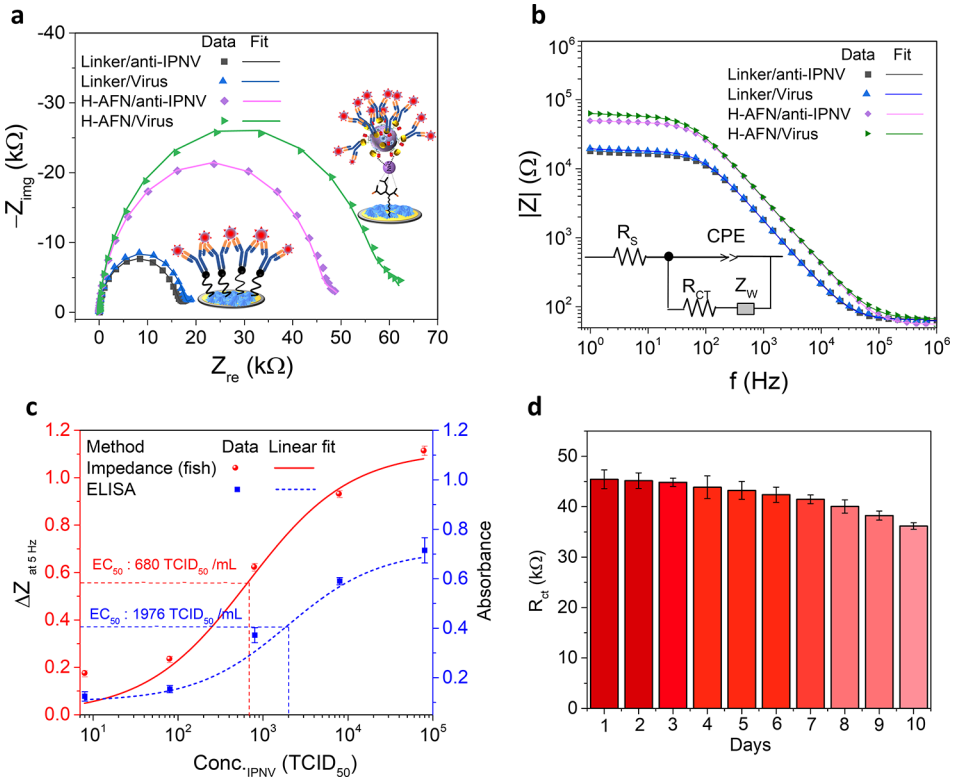

Figure 6. (a) Nyquist and (b) Bode plots representing the sensitivity of the proposed sensor shows the variations in impedance upon binding antibody with H-AFN nanoprobe and antibody on chemical linker for virus bindings; (c) comparison studies of proposed sensor with traditional method (ELISA) show the impedance change and absorbance obtained by ELISA versus different concentrations of IPNV. (d) Change in R_{ct} observation of H-AFN nanoprobe conjugated anti-IPNV sensor to estimate the operational stability of the developed sensor.

fold enhancement in sensitivity for same concentration), which indicated the utilization of H-AFN nanoprobe enhanced the sensitivity of overall sensor performance. The EIS spectra in both methods were fitted to the equivalent circuit, and the extrapolated circuit elements were presented in Table 4 (Supporting Information). Also, operational stability being the primary factors for evaluating the performance of the developed sensor for practical application and thus analyzed anti-IPNV (4.43 mg/mL) coated on disk electrode for 10 days (see in Figure S5, Supporting Information), the sensor still kept in third, sixth, and 10th days in 4 °C after each of its testing show 98.7%, 93.26%, and 81.77%, respectively, no significant change in charge transfer resistant as displayed in Figure 6d.

Apart from high sensitivity and selectivity, the detection of IPNV in the complex biological matrix is an essential factor for the practical feasibility of the developed sensor. Impedance experiments on various concentrations of fish samples on the proposed sensor were performed and compared with standard method ELISA under same concentrations (Figure 6c). The response from ELISA was found to be increasing with increased concentration and the response was fitted with logistic equation as $y = 0.1 + (0.714-0.1)/(1 + (x/1976.1)^{0.8})$ with a correlation coefficient of $R^2 = 0.984$, and EC_{50} of 1976 $TCID_{50}$/mL. The two-sample *t*-test for both null and alternative hypothesis at 0.05 level, at equal variance, does not show any significant difference, and therefore, EIS results showed good correlation with ELISA. Thus, it is expected to utilize the proposed sensor for practical applications. The sensor retained its impedance response for a storage period of 10 days kept at 4 °C. The results indicated that no apparent denaturation occurred and that the Ni-NTA conjugated H-AFN bound surface, which provided an adequate biocompatible environment to preserve the activity of the attached antibodies. Each biosensor was used once for measuring each IPNV concentration, aimed at single-use disposable in vitro applications. The main advantages of the developed impedance-based IPNV sensor over other methods are that it is label-free and inexpensive and requires minimal sample preparation for sensitive detection of the analyte signal.

4. CONCLUSION

In summary, we report on the development of H-AFN nanoprobes as an efficient binding agent of IPNV antibody with enhanced sensitivity toward the detection of IPNV virus. The proposed strategy can be extended to other detection techniques to devise an ultrasensitive and straightforward label-free biosensor. The results demonstrated that H-AFN probe was found to be 12−13 nm from TEM and DLS analysis and provided excellent binding capabilities to IPNV antibodies for the detection of the virus using DPV and EIS methods. To the best of our knowledge, genetically modified H-AFN was used for the first time for the detection of IPNV in salmon fish samples. The sensor exhibited a LOD of 2.69 $TCID_{50}$/mL and possessed a linear range of 100−10000 $TCID_{50}$/mL in both PBS and real fish sample. Furthermore, the sensor also displayed excellent selectivity and sensitivity toward IPNV detection in comparison with traditional linker based EIS methods, which showed three-fold enhancement in *RR*% for the same concentration of the analyte. Also, if the H-AFN subunits expressed with another type of proteins on its surface along with protein-G for binding antibodies, that enabled the

DOI: 10.1021/acs.analchem.9b00187
Anal. Chem. 2019, 91, 5841−5849

development of multiplexed detection system. The proposed H-AFN based electrochemical biosensor provides a simple, inexpensive, and rapid analytical strategy for the identification and validation of IPNV in a fish sample with minimal quantities of analyte volume and preparation. Thus, the proposed biosensor is an attractive candidate for the development of robust bioengineered HAFN expressed platform for the point-of-care and can be widely adopted for the development of EIS biosensors.

■ ASSOCIATED CONTENT

Supporting Information

The Supporting Information is available free of charge on the ACS Publications website at DOI: 10.1021/acs.analchem.9b00187.

H-Apoferritin gene sequence analysis data; constructed human apoferritin gene cloned into pET28b(+); differential pulse voltammetry observation; selectivity test of developed Au electrode for IPNV; H-AFN nanoprobe conjugated anti-IPNV sensor; experimental setup of Au disk electrode system; experimental fit values; comparison of selected quantities measured from various sensing methods towards IPNV detection; values of the equivalent circuit elements obtained (PDF)

■ AUTHOR INFORMATION

Corresponding Authors

*E-mail: mhlee7@cau.ac.kr. Phone: +82-2-820-5503. Fax: +82-2-814-2651.

*E-mail: junmin@cau.ac.kr. Phone: +82-2-820-5348. Fax: +82-2-814-2651.

ORCID

Min-Ho Lee: 0000-0002-7028-4745

Author Contributions

‡S.G.C. and A.K.Y. contributed equally to this work.

Notes

The authors declare no competing financial interest.

■ ACKNOWLEDGMENTS

We are gratefully acknowledged for this work was funded by the Ministry of Trade, Industry, and Energy of Korea (Grant Nos. 10062995 and 20000580).

■ REFERENCES

(1) Saint-Jean, S. R.; Borrego, J. J.; Perez-Prieto, S. I. *Adv. Virus Res.* **2003**, *62*, 113−165.

(2) Ronneseth, A.; Haugland, G. T.; Wergeland, H. I. *Fish Shellfish Immunol.* **2013**, *34*, 1294−1305.

(3) Roberts, R. J.; Pearson, M. D. *J. Fish Dis.* **2005**, *28*, 383−390.

(4) Julin, K.; Johansen, L. H.; Sommer, A. I.; Jorgensen, J. B. *J. Fish Dis.* **2015**, *38*, 1005−1019.

(5) Dadar, M.; Memari, H. R.; Vakharia, V. N.; Peyghan, R.; Shapouri, M. S. A.; Mohammadian, T.; Hasanzadeh, R.; Ghasemi, M. *Fish Shellfish Immunol.* **2015**, *47*, 390−396.

(6) Bello-Pérez, M.; Falcó, A.; Galiano, V.; Coll, J.; Perez, L.; Encinar, J. A. *Drug Des., Dev. Ther.* **2018**, *12*, 2337.

(7) Houston, R. D.; Haley, C. S.; Hamilton, A.; Guy, D. R.; Tinch, A. E.; Taggart, J. B.; Mc Andrew, B. J.; Bishop, S. C. *Genetics* **2008**, *178*, 1109.

(8) Hill, B.; Way, K. *Annual Review of Fish Diseases.* **1995**, *5*, 55−77.

(9) Cho, I. H.; Irudayaraj, J. *Int. J. Food Microbiol.* **2013**, *164*, 70−75.

(10) Ronkainen, N. J.; Halsall, H. B.; Heineman, W. R. *Chem. Soc. Rev.* **2010**, *39*, 1747−1763.

(11) Wei, T. X.; Tu, W. W.; Zhao, B.; Lan, Y. Q.; Bao, J. C.; Dai, Z. H. *Sci. Rep.* **2015**, *4*, 4.

(12) Yagati, A. K.; Chavan, S. G.; Baek, C.; Lee, M.-H.; Min, J. *Sensors* **2018**, *18*, 18.

(13) Baek, S. H.; Kim, M. W.; Park, C. Y.; Choi, C.-S.; Kailasa, S. K.; Park, J. P.; Park, T. J. *Biosens. Bioelectron.* **2019**, *123*, 223−229.

(14) Costanzo, F.; Colombo, M.; Staempfli, S.; Santoro, C.; Marone, M.; Frank, R.; Delius, H.; Cortese, R. *Nucleic Acids Res.* **1986**, *14*, 721−736.

(15) Ma-Ham, A.; Wu, H.; Wang, J.; Kang, X.; Zhang, Y.; Lin, Y. *J. Mater. Chem.* **2011**, *21*, 8700−8708.

(16) Wang, M.; Yin, H. S.; Fu, Z. L.; Guo, Y. L.; Wang, X. X.; Zhou, Y. L.; Ai, S. Y. *J. Solid State Electrochem.* **2014**, *18*, 2829−2835.

(17) Zhen, Z.; Tang, W.; Chen, H.; Lin, X.; Todd, T.; Wang, G.; Cowger, T.; Chen, X.; Xie, J. *ACS Nano* **2013**, *7*, 4830−4837.

(18) Ma-Ham, A. H.; Wu, H.; Wang, J.; Kang, X. H.; Zhang, Y. Y.; Lin, Y. H. *J. Mater. Chem.* **2011**, *21*, 8700−8708.

(19) Guss, B.; Eliasson, M.; Olsson, A.; Uhlen, M.; Frej, A.; Jörnvall, H.; Flock, J.; Lindberg, M. *EMBO J.* **1986**, *5*, 1567−1575.

(20) Hwang, M. P.; Lee, J.-W.; Lee, K. E.; Lee, K. H. *ACS Nano* **2013**, *7*, 8167−8174.

(21) Heger, Z.; Skalickova, S.; Zitka, O.; Adam, V.; Kizek, R. *Nanomedicine* **2014**, *9*, 2233−2245.

(22) Ataka, K.; Giess, F.; Knoll, W.; Naumann, R.; Haber-Pohlmeier, S.; Richter, B.; Heberle, J. *J. Am. Chem. Soc.* **2004**, *126*, 16199−16206.

(23) Liao, T.; Yuan, F.; Yu, H.; Li, Z. *Anal. Methods* **2016**, *8*, 1577−1585.

(24) Dali, M.; Zinoubi, K.; Chrouda, A.; Abderrahmane, S.; Cherrad, S.; Jaffrezic-Renault, N. *J. Electroanal. Chem.* **2018**, *813*, 9−19.

(25) Yagati, A. K.; Park, I.; Cho, S.; Min, J. *Sci. Adv. Mater.* **2017**, *9*, 1595−1602.

(26) Yagati, A. K.; Pyun, J. C.; Min, J.; Cho, S. *Bioelectrochemistry* **2016**, *107*, 37−44.

(27) Yagati, A. K.; Choi, Y.; Park, J.; Choi, J. W.; Jun, H. S.; Cho, S. *Biosens. Bioelectron.* **2016**, *80*, 307−314.

(28) Hayashi, Y.; MATSUDA, R.; Ito, K.; NISHIMURA, W.; IMAI, K.; MAEDA, M. *Anal. Sci.* **2005**, *21*, 167−169.

(29) Valentin, M. A.; Ma, S. L.; Zhao, A.; Legay, F.; Avrameas, A. *J. Pharm. Biomed. Anal.* **2011**, *55*, 869−877.

DOI: 10.1021/acs.analchem.9b00187
Anal. Chem. 2019, 91, 5841−5849